Electronic Supplementary Material (ESI) for Journal of Materials Chemistry C.

Supporting Information

Simple Excited-State Modification toward Deep-Blue Hybridized Local and Charge-Transfer (HLCT) Fluorophore and Non-doped Organic Light-Emitting Diodes

Yumiao Huo[a,d], Jichen Lv[a], Minghao Wang[a], Zuning Duan[a], Haoyuan Qi[a], Shengnan Wang[a], Yuchao Liu[a], Ling Peng[b], Shian Ying[a*] and Shouke Yan[a,c*]

[a] Key Laboratory of Rubber-Plastics, Ministry of Education, School of Polymer Science and Engineering, Qingdao University of Science and Technology, Qingdao 266042, P. R. China.

[b] College of Chemistry and Chemical Engineering, Heze University, Heze 274015, P. R. China.

[c] State Key Laboratory of Chemical Resource Engineering, College of Materials Science and Engineering, Beijing University of Chemical Technology, Beijing 100029, P. R. China.

[d] College of Materials Science and Engineering, Shandong University of Science and Technology, Qingdao 266590, P. R. China.

*Corresponding author: shian0610@126.com (S. Ying); skyan@mail.buct.edu.cn (S. Yan)

Experimental Section

1. Experimental measurements

^{1}H and ^{13}C NMR spectra of target materials were performed by a Bruker AVAN CE NEO 400 spectrometer with tetramethyl silane (TMS) as the internal standard in $CDCl_3$ at room temperature. Mass spectra (MS) were carried out by a high-resolution quadrupole time of flight tandem mass spectrometer (TOF-MS) operating in MALDI-TOF mode. UV-vis absorption and emission spectra in solution and neat films were recorded by HITACHI U-4100 Spectrophotometer and Hitachi F-7000 Fluorescence Spectrophotometer, respectively. Photoluminescence quantum yields (PLQYs) were measured using in an integration sphere setup (Hamamatsu C11347-11) equipped with a xenon high-pressure lamp and a multichannel analyzer from 200 to 950 nm. Transient fluorescence spectra were determined on the Edinburgh FLS1000 Photoluminescence Spectrometer. Low temperature phosphorescence and fluorescence spectra of target compounds was measured at 77 K in toluene solution by the Hitachi F-7000 Fluorescence Spectrophotometer. Thermogravimetric analysis (TGA) curve of compound was recorded by using a Netzsch (209F1) thermogravimetric analyzer under a nitrogen atmosphere (50 mL min^{-1}) at a heating rate of 10 ^{o}C min^{-1}. Differential scanning calorimetry (DSC) curves of target compounds were recorded by a Netzsch DSC (204F1) instrument at a heating (or cooling) rate of 10 ^{o}C min^{-1}. The highest occupied molecular orbital (HOMO) energy level of the target compound was measured on a CHI760D electrochemical workstation via using cyclic voltammetry (CV) with a glass carbon disk as the working electrode, a platinum wire as the counter electrode, an Ag/Ag^{+} electrode as the reference electrode, and ferrocene as the standard reference. The material was dissolved in anhydrous dichloromethane solution with 0.1 mol L^{-1} Bu4NPF6 as the electrolyte to measure the oxidation, from which the HOMO energy level was estimated by the formalism: HOMO = - (E_{ox} vs. Fc^{+}/Fc + 4.8) eV, where E_{ox} vs. Fc^{+}/Fc is oxidation onset potential relative to Fc^{+}/Fc reference. The lowest unoccupied molecular orbital (LUMO) energy level was calculated from the difference between the HOMO energy level and optical bandgap (E_{og}) which was estimated from onsets of the UV-Vis spectrum in THF.

2. Device fabrication and measurement

Patterned indium-tin-oxide (ITO) glasses were ultrasonically treated in detergents and deionized water, then dried at 120 °C for 30 min. After treated by oxygen plasma, ITO-substrates were transferred into the vacuum deposition system. The devices were fabricated under the pressure of $< 2 \times 10^{-4}$ Pa. The evaporation rates were detected by a frequency counter and calibrated by a Dektak 6 M profiler (Veeco). Organic materials, lithium fluoride (LiF) and aluminum (Al) were thermally evaporated at the rates of 1-1.5, 0.2 and 5-10 Å s^{-1} via a shadow

mask. The emitting region of devices was 3 × 3 mm^2 that determined by the overlap between ITO and Al electrodes. The current density–luminance–voltage characteristics of devices were recorded by a constant source of Keithley 2450 source meter and LS160 luminance meter. EL spectra were recorded by using an optical analyzer FlAME-S-VIS-NIR photometer. Supposing the light emitted by OLEDs is in accord with the Lambertian distribution, the EQEs can be estimated from the EL spectra, luminance, and current density.

3. Theoretical calculations

All the density functional theory (DFT) and time dependent DFT (TDDFT) calculations of target materials were performed by using Gaussian 09 package. The optimized ground-state geometries, energy levels, and frontier molecular orbital (FMO) distributions were calculated on the basis of DFT by using B3LYP/6-31G(d) method. According to the TDDFT calculation, the optimized excited-state geometries, natural transition orbitals (NTOs), singlet and triplet state energies, and oscillator strength were carried out based on B3LYP/6-31G(d) method.

4. Synthesis and characterization of target materials

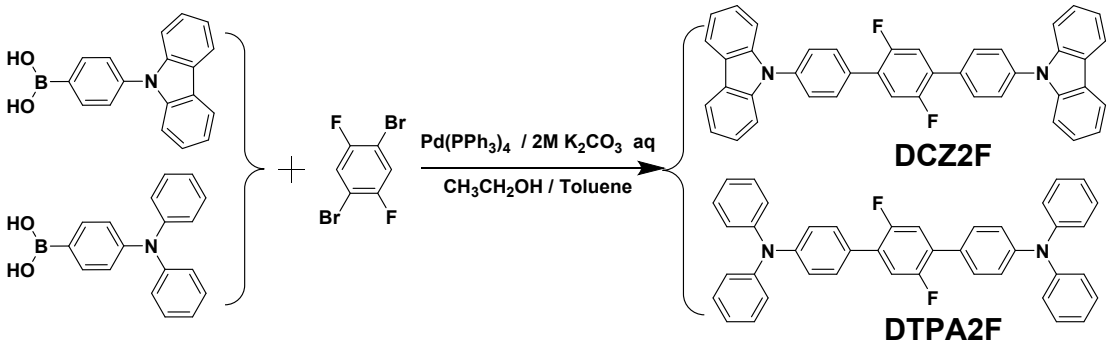

Scheme S1. Synthetic Routes to DCZ2F and DTPA2F.

Synthesis of 9,9'-(2',5'-difluoro-[1,1':4',1''-terphenyl]-4,4''-diyl)bis(9H-carbazole) (DCZ2F)

In N_2 atmosphere, 1,4-dibromo-2,5-difluorobenzene (1.35 g, 5 mmol), (4-(9*H*-carbazol-9-yl)phenyl)boronic acid (3.16 g, 11 mmol) and tetrakis-triphenylphosphine palladium $Pd(PPh_3)_4$ (0.29 g, 0.25 mmol) were added into the two-neck round-bottom flask. Then 2M potassium carbonate solution (10 mL), CH_3CH_2OH (10 mL) and toluene (30 mL) were injected into flask using syringes. After refluxed for 24 h, the reaction mixture was cooled down to room temperature. Then the mixture was extracted three times by dichloromethane, and the organic phase was dried over anhydrous magnesium sulfate. After filtration and evaporation, the crude product was further purified by silica-gel column chromatography using dichloromethane/ petroleum (1/10, v/v) as the solvent and finally prepared by recrystallization using the mixed solvent of dichloromethane and ethanol to give a white solid (2.45 g, yield: 82%). ^1H NMR (400 MHz, $CDCl_3$, δ ppm):

8.18 (d, J = 8.1 Hz, 4H), 7.87 (d, J = 8.2 Hz, 4H), 7.72 (d, J = 8.0 Hz, 4H), 7.57 – 7.50 (m, 4H), 7.50 – 7.40 (m, 6H), 7.37 – 7.29 (m, 4H). ^{13}C NMR (101 MHz, $CDCl_3$ δ ppm): 140.84, 137.99, 133.49, 130.50, 128.67, 127.64, 127.30, 126.21, 123.71, 120.54, 120.34, 120.23, 109.97. HRMS (ESI, m/z) calcd for C42H26F2N2: 596.2064; $[M + H]^+$ found: 597.2137.

Synthesis of 2',5'-difluoro-N⁴,N⁴,N⁴'',N⁴''-tetraphenyl-[1,1':4',1''-terphenyl]-4,4''-diamine (DTPA2F)

The compound DTPA2F was synthesized according to the similar procedure as for *DCZ2F* by using (4-(diphenylamino)phenyl)boronic acid (3.18 g, 11 mmol) instead of (4-(9*H*-carbazol-9-yl)phenyl)boronic acid. And DTPA2F was obtained as white solid (Yield: 2.60 g, 86.7%). ^{1}H NMR (400 MHz, $CDCl_3$, δ ppm): 7.41 (d, *J* = 6.4 Hz, 4H), 7.27 – 7.21 (m, 8H), 7.17 (t, *J* = 9.0 Hz, 2H), 7.14 – 7.05 (m, 12H), 7.02 (t, *J* = 7.3 Hz, 4H). ^{13}C NMR (101 MHz, $CDCl_3$ δ ppm): 147.96, 147.58, 129.68, 129.66, 129.65, 129.51, 128.14, 124.96, 123.46, 123.02. HRMS (ESI, m/z) calcd for C42H30F2N2: 600.2377; $[M + H]^+$ found: 601.2450.

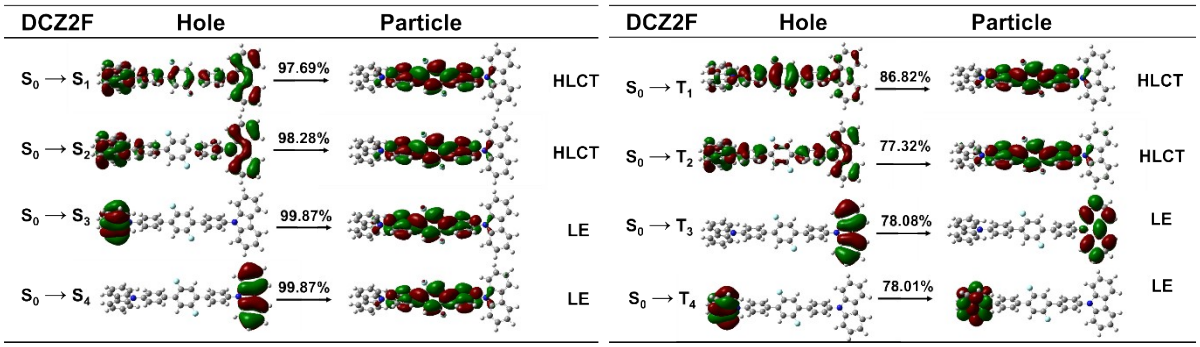

Fig. S1. The natural transition orbitals (NTOs) of the singlet ($S_{1\text{-}4}$) and triplet ($T_{1\text{-}4}$) excited states using the Gaussian 09 package at the basis set of RB3LYP/ 6-31G(d).

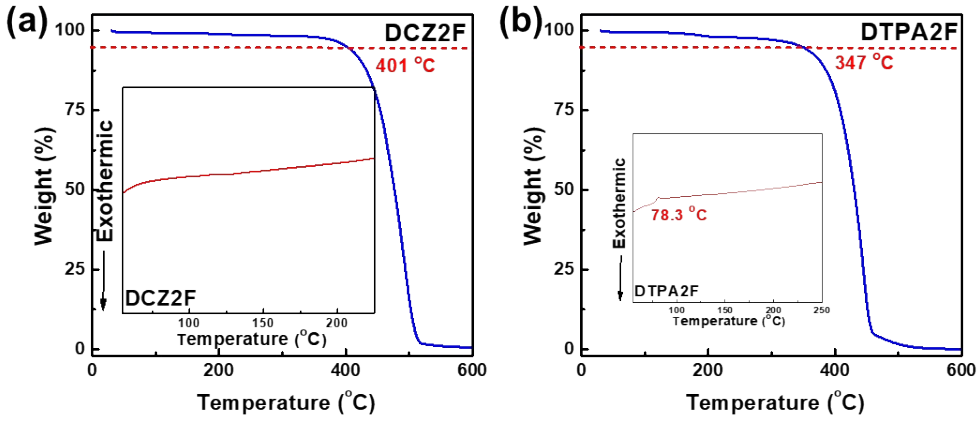

Fig. S2. TGA curves of DCZ2F (a) and DTPA2F (b). Insert: DSC curves of DCZ2F and DTPA2F.

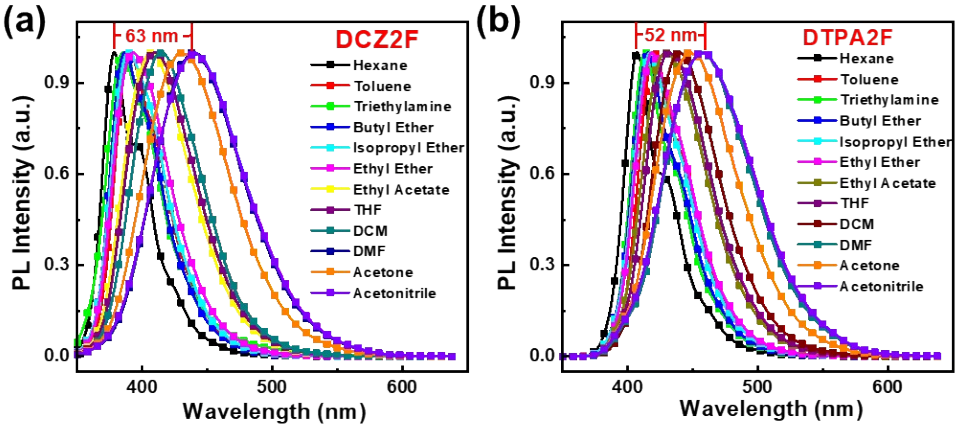

Fig. S3. PL spectra of DCZ2F (a) and DTPA2F (b) in different solvents with the concentrations of 10 μM.

Detailed Lippert-Mataga Calculation

The Stokes shift ($\nu_A - \nu_{PL}$) versus orientational polarizability ($f(\varepsilon,n)$) of solvents can be constructed by the Lippert-Mataga model with the Equation 1 as below.

$$hc(\nu_A - \nu_{PL}) = hc(\nu_A^0 - \nu_{PL}^0) + \frac{2(\mu_e - \mu_g)^2}{a_0^3} f(\varepsilon,n) \quad (1)$$

Here, h is the Plank constant, c is the light speed in vacuum, μ_g and μ_e are the ground-state excited-state dipole moments, $f(\varepsilon,n)$ is the orientational polarizability of solvents, a_0 is the Onsager cavity radius, $\nu_A^0 - \nu_{PL}^0$ is the Stokes shifts when f is zero, respectively.

Take differential on both sides of the Equation 1, the Equation 2 can be obtained:

$$\mu_e = \mu_g + \{\frac{hca_0^3}{2} \times [\frac{d(\nu_A - \nu_{PL})}{df(\varepsilon,n)}]\}^{1/2} \quad (2)$$

$f(\varepsilon,n)$ and a_0 can be obtained by the Equation 3 and 4:

$$f(\varepsilon,n) = \frac{\varepsilon - 1}{2\varepsilon + 1} + \frac{n^2 - 1}{2n^2 + 1} \quad (3)$$

$$a_0 = (\frac{3M}{4\pi Nd})^{1/3} \quad (4)$$

Where, ε and n are dielectric constant and refractive index of solvent, N is Avogadro's number, M is molar mass, and d is density of the solvents, respectively. The values of (ε, n) and a_0 can be estimated by the Equation 3 and 4. The μ_g of DCZ2F (0.058 D) were estimated with the Gaussian 09 package at the level of B3LYP/6-31G(d). The $\frac{d(\nu_A - \nu_{PL})}{df(\varepsilon,n)}$ can be estimated with the solvatochromic experiment data listed in Table S1. With the information above, DCZ2F shows two section lines with the μ_es of 11.22 and 21.66 D in low- and high-polar solvents.

Table S1. The detailed absorption and emission data of **DCZ2F** in different solvents.

Solvents	ε	n	f(ε, n)	λ_A (nm)	λ_{PL} (nm)	ν_A- ν_{PL} (cm^{-1})
Hexane	1.9	1.375	0.0012	328	378	4032.778423
Toluene	2.38	1.494	0.013	328	390	4846.779237
Triethylamine	2.42	1.401	0.048	328	384	4446.138211
Butyl ether	3.08	1.399	0.096	328	386	4581.069127
Isopropyl ether	3.88	1.368	0.145	328	390	4846.779237
Ethyl ether	4.34	1.352	0.167	328	393	5042.512257
Ethyl acetate	6.02	1.372	0.2	328	405.6	5832.972531
Tetrahydrofuran	7.58	1.407	0.21	328	410	6097.560976
Dichloromethane	8.93	1.424	0.217	328	415	6391.419336
Dimethylformamide	37	1.427	0.276	328	437	7604.509684
Acetone	20.7	1.359	0.284	328	430	7231.990925
Acetonitrile	37.5	1.344	0.305	328	441	7812.067917

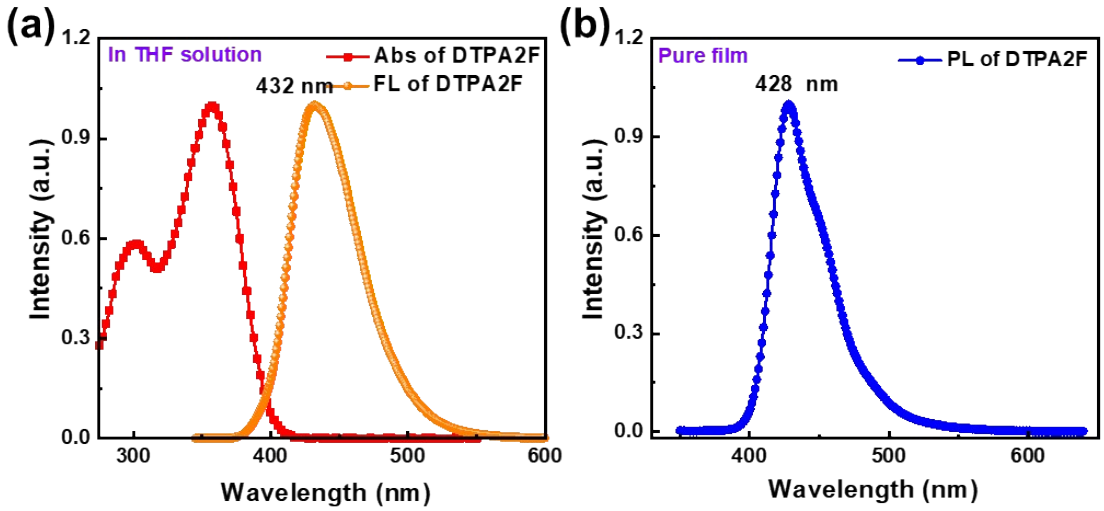

Fig. S4. (a) The UV-vis absorption and emission spectra of DTPA2F in the THF solution (10 μM). (b) Emission spectra of DTPA2F in the neat film.

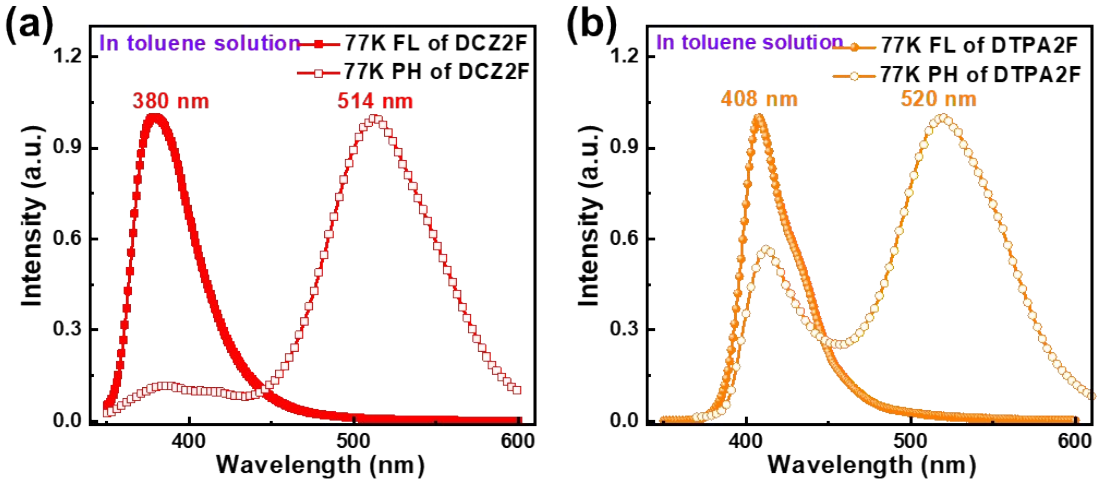

Fig. S5. Low temperature fluorescence and phosphorescence spectra of DCZ2F (a) and DTPA2F (b) in the toluene solution.

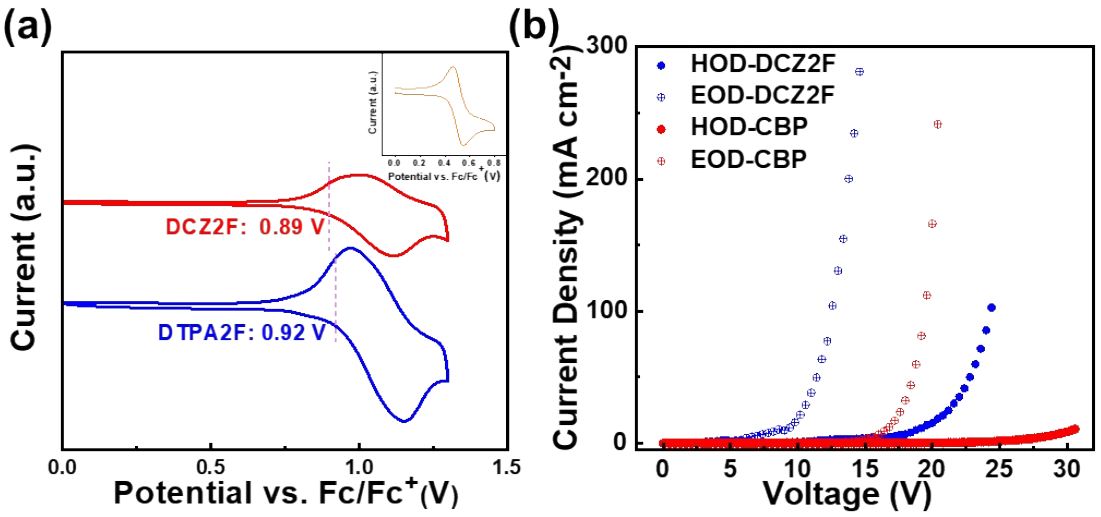

Fig. S6. (a) Cyclic voltammograms curves of DCZ2F and DTPA2F. (b) The current density-voltage curves of electron- and hole-only devices (EOD, HOD) for DCZ2F and CBP.

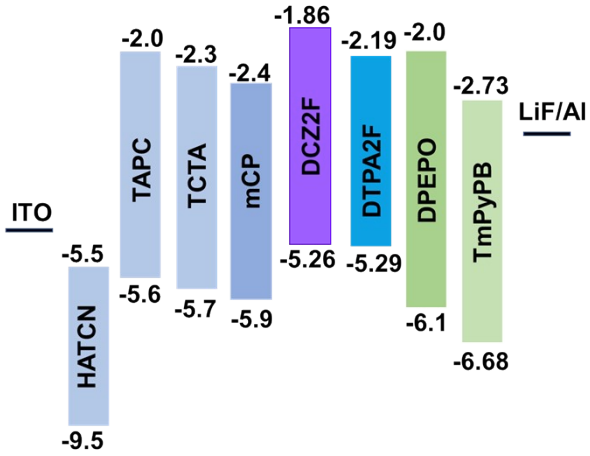

Fig. S7. The energy level diagram of materials used in the OLEDs.

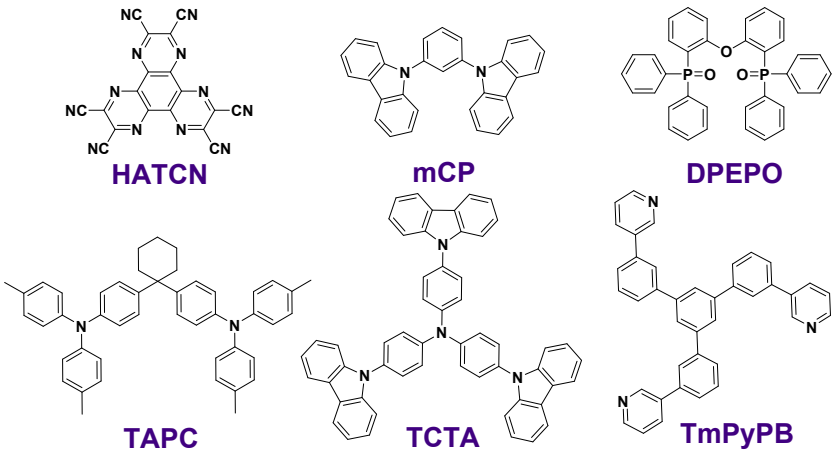

Fig. S8. The molecular structure of organic materials used in the OLEDs.

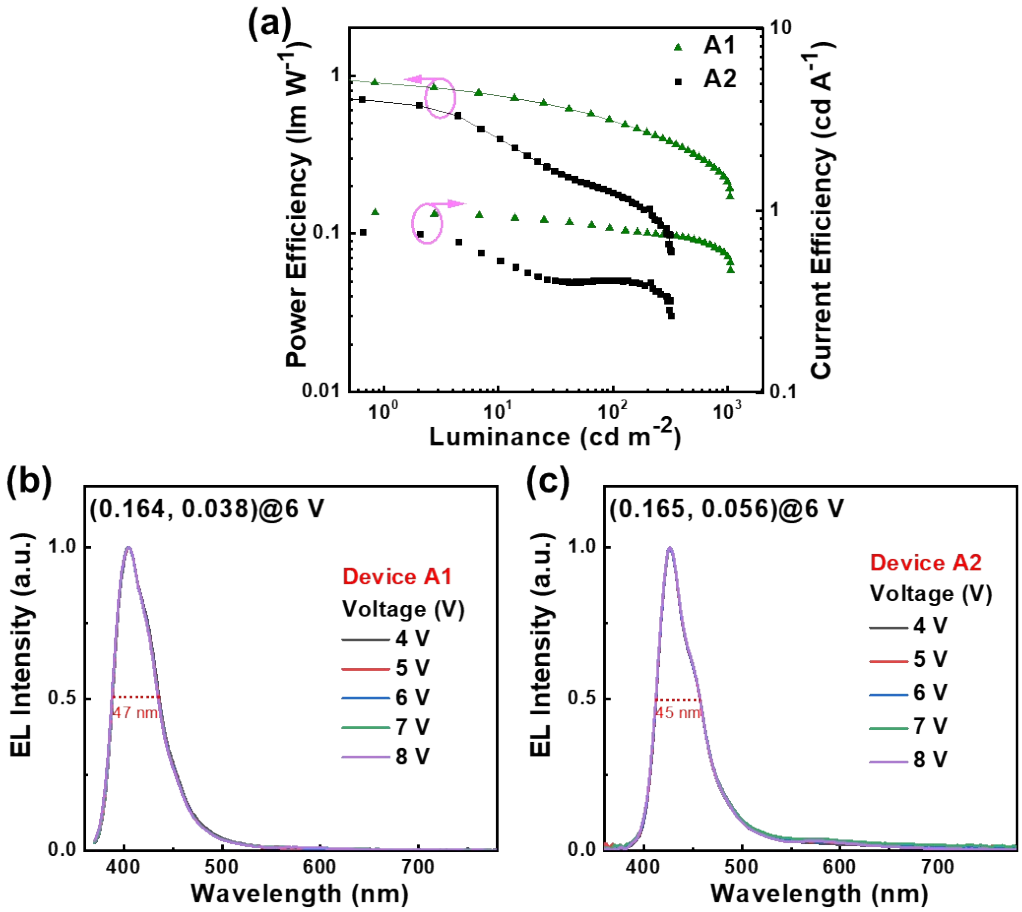

Fig. S9. (a) Power efficiency-luminance-current efficiency curves of the devices **A1** and **A2**. (b) EL spectra of the device **A1** at the applied voltages from 4 to 8 V. (c) EL spectra of the device **A2** at the applied voltages from 4 to 8 V.

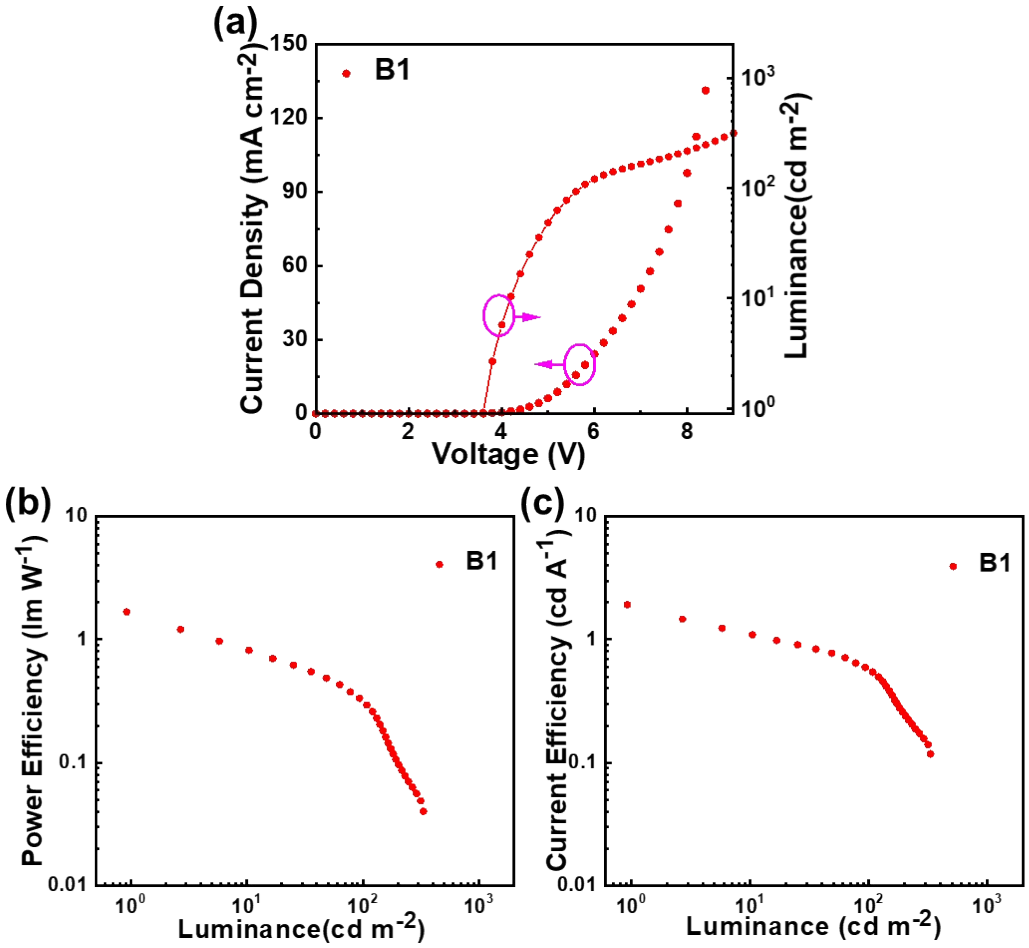

Fig. S10. (a) Current density–voltage–luminance curves of the device **B1**. (b) Power efficiency-luminance curve of the device **B1**. (c) Current efficiency-luminance curve of the device **B1**.